Journal of Vacuum Science and Technology B

RESEARCH ARTICLE | APRIL 23 2024

Planar microcoil arrays for *in vitro* cellular-level micromagnetic activation of neurons

Renata Saha ; Onri J. Benally ; Sadegh Faramarzi ; Robert Bloom ; Kai Wu ; Denis Tonini ; Maple Shiao; Susan A. Keirstead ; Walter C. Low ; Theoden I. Netoff ; Jian-Ping Wang

J. Vac. Sci. Technol. B 42, 033001 (2024)
https://doi.org/10.1116/6.0003362
CHORUS

JVST B
Journal of Vacuum Science & Technology B

ARTICLE

pubs.aip.org/avs/jvb

Planar microcoil arrays for *in vitro* cellular-level micromagnetic activation of neurons

Cite as: J. Vac. Sci. Technol. B **42**, 033001 (2024); doi: 10.1116/6.0003362
Submitted: 5 December 2023 · Accepted: 4 March 2024 ·
Published Online: 23 April 2024

Renata Saha,[1] Onri J. Benally,[1] Sadegh Faramarzi,[2] Robert Bloom,[1] Kai Wu,[1] Denis Tonini,[1] Maple Shiao,[3] Susan A. Keirstead,[4,5] Walter C. Low,[3,4,5] Theoden I. Netoff,[2] and Jian-Ping Wang[1,a)]

AFFILIATIONS

[1]Department of Electrical and Computer Engineering, University of Minnesota, Minneapolis, Minnesota 55455
[2]Department of Biomedical Engineering, University of Minnesota, Minneapolis, Minnesota 55455
[3]Department of Neurosurgery, University of Minnesota, Minneapolis, Minnesota 55455
[4]Stem Cell Institute, University of Minnesota, Minneapolis, Minnesota 55455
[5]Department of Integrative Biology and Physiology, University of Minnesota, Minneapolis, Minnesota 55455

[a)]**Author to whom correspondence should be addressed:** jpwang@umn.edu

ABSTRACT

In the treatment of neurodegenerative disorders, a potential cure at a single neuron cell resolution is still lacking. Micromagnetic neurostimulation, although in its infancy, is one of the most promising techniques that offer spatially selective activation of neurons through micrometer-sized coils or microcoils (μcoils). Time-varying current drives these μcoils and generates a time-varying magnetic field which in turn induces an electric field to activate the neural tissues. In this work, we report the design and fabrication of planar μcoil arrays, termed Magnetic Patch (MagPatch), for activating single neurons. Using numerical calculations on ANSYS-Maxwell and NEURON, we report an optimized MagPatch array design that exploits the directionality of the induced electric field from the μcoils to enhance spatial selectivity. Each μcoil has an outer dimension of $190 \times 190\,\mu m^2$ and one MagPatch array contains 8 μcoils. For proof-of-concept design and development, the MagPatch array has been fabricated on Si-substrates using Ti, Au, and Si_3N_4 to ensure preliminary biocompatibility. They were then encapsulated in Parylene-C, a waterproof, anti-leakage current coating, thereby ensuring basic surface biocompatibility. Human neuroblastoma cells were cultured directly on the surface encapsulated MagPatch, and calcium fluorescence imaging was used to assess cell functionality. The impact of scaling the dimensions of the μcoil in the MagPatch array on electrical characteristics, Q-factor, and thermal effects on neural tissues from these μcoils have also been discussed.

I. INTRODUCTION

It has been a little over a decade since the first experimental demonstration of micromagnetic neurostimulation was made.[1] In that work, Bonmassar *et al.*[1] used commercially available solenoidal μcoils to activate rabbit retinal neurons in an *in vitro* experimental setting. Since then, reports for new and efficient designs for micromagnetic stimulators have rarely been reported. However, the commercially available solenoidal μcoil has been extensively used in several *in vitro*[2] and *in vivo*[3–5] experiments. They portrayed several unique features of micromagnetic stimulation such as orientation dependence of the μcoil, importance of directionality of the induced electric field in successful neurostimulation, distance dependence, dose-response relationship for micromagnetic stimulation (μMS), etc.[2,3,5–8] In a recent work, Saha *et al.*[9] reported that both circular helix-shaped μcoil and rectangular helix-shaped μcoil are significantly more efficient for μMS when compared to solenoid-shaped μcoil. However, to date, only a limited number of attempts have been made to design and fabricate new shapes for μcoils in μMS. Special mention includes the works of Lee *et al.*[4] where they fabricated a single loop V-shaped μcoil for intracortical stimulation, Rizou and Prodromakis[10] where they fabricated a 6×6 planar μcoil array for cellular-level neurostimulation, Jeong *et al.*[11] where they fabricated planar μcoils in Fig. 8 for ultra-focal μMS, and Khalifa *et al.*[12] where they reported the microfabrication of solenoids with FeGaB/Al_2O_3 cores for precise control of neuronal populations through μMS. Yet the need for improved designs of

custom fabricated μcoils in μMS is still active for various reasons as follows. The single loop V-shaped μcoil has been reported to successfully activate both L5 pyramidal neurons as well as intracortical neurons.[4,13,14] However, Alzahrani and Roth[15] recently raised concerns about the nature of neurostimulation from the designed V-shaped μcoil being entirely micromagnetic. They provided sufficient numerical evidence that the single loop V-shaped μcoil of the reported dimensions was not able to generate the induced electric field threshold necessary for the successful activation of the neuron.[15] In addition, the μcoil in Ref. 4 was made of copper which is cytotoxic and must be avoided in any biomedical implant.[16] Similar concerns can be raised for the microfabricated solenoid with FeGaB/Al_2O_3 core[12] as the bulk biocompatibility of the material of the core is questionable when considering the prototype for a neural implant. Finally, the design for the planar μcoils in Fig. 8 (Ref. 11) and the 6×6 planar μcoil array[10] reported were never tested for neurostimulation capability in a neural tissue environment.

Therefore, the reports on customized μcoil fabrication for μMS lack two important features. First, the design and development of a bulk biocompatible prototype could trigger cellular-level neurostimulation. Second, a study on the impact of μcoil arrays in micromagnetic neurostimulation in addition to how the directionality of the induced electric field from each of the μcoils in the array affects neurostimulation performance. This motivated the design and fabrication of the Magnetic Patch (MagPatch), a rectangular helix-shaped μcoil array in this work. The prototype was fabricated on a silicon substrate using three materials—titanium (Ti), gold (Au), and silicon nitride (Si_3N_4) (see Sec. II A). The complete MagPatch prototype is encapsulated in a water-tight, biocompatible, and insulating coating—Parylene-C (see Sec. II B). All three materials have been used previously in medical implants.[17–19] Overall, the MagPatch array has been designed as per "The Pentagon for Implant Design Constraints" reported by McGlynn *et al.*[20] The μcoils in the designed MagPatch array have been numerically studied using a NEURON (https://www.neuron.yale.edu/neuron/) model[21] to facilitate single neuron activation (see Secs. IV A and IV B). Furthermore, the impact of directionality of the induced electric field from each of the μcoils in the array on successful neurostimulation performance has been studied in detail (see Secs. IV A and IV B). Combining finite element modeling (FEM) (see Sec. III A) and NEURON (see Sec. III B) models, a strength-frequency curve for a single μcoil in the MagPatch has been reported (see Sec. IV D). Finally, preliminary testing to address potential biocompatibility concerns for MagPatch has been demonstrated *in vitro* by culturing the SHSY5Y human neuroblastoma cell line (see Sec. IV E). The cultured neuroblastoma cells showed calcium concentration changes when an external chemical stimulus was applied. This implied the cells were alive in the fabricated MagPatch environment. The impact of scaling on the μcoils in the MagPatch array on electrical characteristics, Q-factor, and thermal effects on neural tissues has also been studied.

II. EXPERIMENT

A. Fabrication of the MagPatch array

Bare silicon substrates are diced into $4 \times 2\ cm^2$ rectangles [see Fig. 1(a)]. The fabrication of the planar μcoils begin with a partial stack of evaporated Ti (25 nm)/Au (250 nm)/Ti (15 nm) on a bare Si/SiO_2 wafer. This is followed by plasma-enhanced chemical vapor

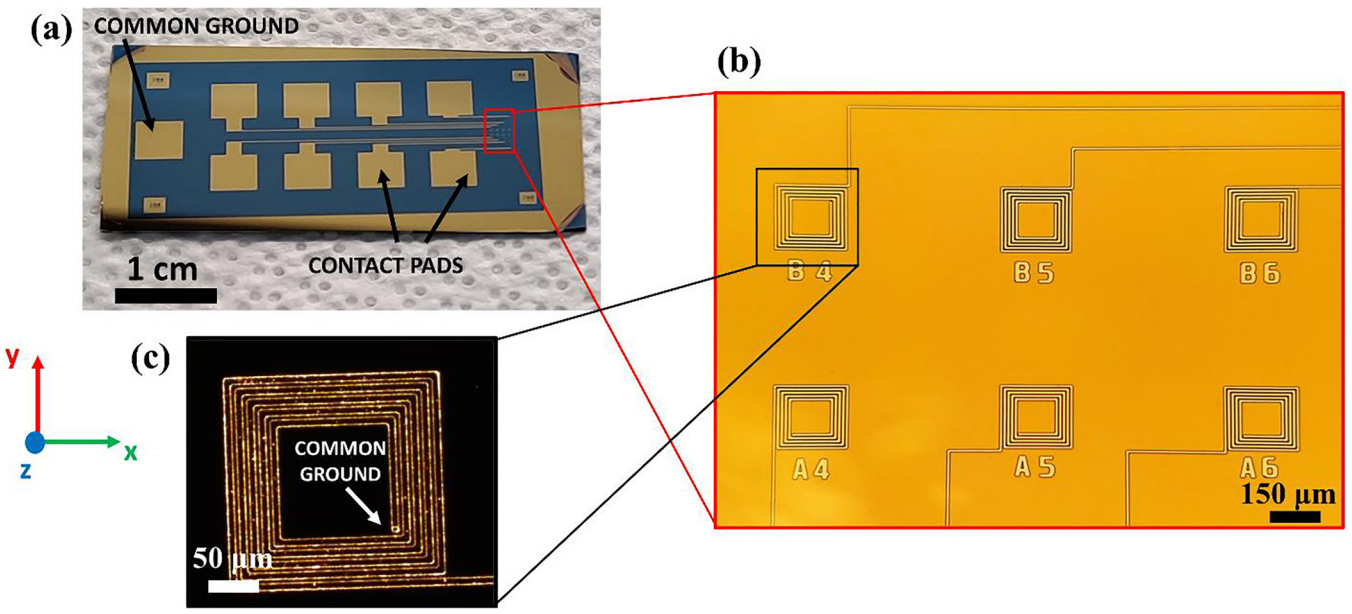

FIG. 1. MagPatch array. (a) The complete device. (b) Optical microscope image of the arrays of microcoil at the tip showing six out of eight μcoils at the tip. (c) Single μcoil.

deposition of 100 nm thick Si_3N_4 at 200 °C. This Si_3N_4 layer forms the passivation layer between the ground and the contact pads. Following this is the first step of photolithography to expose the ground contacts, whereas the remaining area of the device will be masked by the photoresist. Next, the 100 nm Si_3N_4 layer over the ground contacts is ion mill etched using the negative photoresist as the masking layer for the remaining area of the device. Calibrating the ion mill etch rate is the most critical step for this device's fabrication. An under-etch might cause a passivation layer to remain on the ground contacts, which is undesired. An over-etch might cut deep into the 250 nm Au layer as the ion mill etch rate for Au is greater than that of Si_3N_4.[22] Ion mill etch is followed by evaporation of 10 nm Ti and 100 nm of Au in those exposed ground contacts followed by lift-off of Au. The next step is to perform the photolithography for the μcoil patterns and the contact pads as in Fig. 1(b). Following this, 50 nm of Ti and 200 nm of Au are evaporated. While this 200 nm of Au forms the seed layer for the electroplating of ∼2 μm of Au in Fig. S1 (see S1 in the supplementary material),[38] the 50 nm Ti is added to improve the adhesion of the Au layer to the Si_3N_4 passivation layer. Prior to electroplating, the previous Ti and Au layers are lifted off followed by a tape test. Only those devices which passed the tape test are electroplated. At this stage, the fabrication of the Au μcoil array is complete.

The entire microfabrication flowchart for MagPatch arrays is depicted in Fig. S1 (see S1 in the supplementary material).[38] The fabricated MagPatch arrays were imaged using an optical microscope [see Figs. 1(a)–1(c)] as well as by scanning electron microscope [see Fig. S2(a) and S2(b)]. The electrical characteristics and LCR parameters of the μcoil were calculated using numerical methods and validated using LCR meter (Model No. BK Precision 889B) measurements (see S4 in the supplementary material).[38]

B. Packaging and electrical interfacing of the μcoils

The goal for fabricating these μcoils was to study micromagnetic stimulation on neuron cell cultures. Hence, while fabricating these implants, there are very few materials that could be used. The MagPatch array is primarily made of Ti, Au, and Si_3N_4—all three materials are being used in existing medical implants.[17–19] Therefore, preliminary biocompatibility of the entire MagPatch array has been ensured. However, while fabricating these micromagnetic implants, it is of utmost importance to ensure that the device has no leakage current. Therefore, encapsulating the device with a biocompatible, water-tight polymer constitutes a very important step in its packaging. In this work, we used a 10 μm thick layer of Parylene-C as an anti-leakage current coating for the MagPatch arrays. This coating was applied through physical vapor deposition of Parylene-C dimers using the SCS-Labcoater Parylene-C deposition system. However, Parylene-C does not adhere well to the metallic and dielectric layers (Ti, Au, and Si_3N_4) of our MagPatch device.[23] Therefore, we coated the device with an A-174 silane adhesion promoter for better adherence to Parylene-C. This A-174 adhesion promoter introduced a methacrylate group to the surface of the μcoils that acted as a coupling agent to the Parylene-C.[24] Only the μcoils at the tip were encapsulated with Parylene-C, the contact pads were not [see Fig. S2(c) in S2 in the supplementary material].[38]

The electrical connections from the MagPatch array to the external driving circuit were achieved by soldering 28 AWG solid wires directly to the contact pads. The soldered wires were connected to the external driving circuitry using alligator clips. The whole device was then glued to a fiberglass plate to fit the calcium fluorescence imaging scope experimental setup discussed in Sec. II D. The neuroblastoma cells would be cultured only on the Parylene-C coated region, i.e., at the tip of the MagPatch. Hence, to form an isolated region where the cells can be grown, a polypropylene chamber was 3D-printed and adhered surrounding the μcoil array at the tip using polydimethylsiloxane [see Fig. S2(d) in S2 in the supplementary material].[38] Finally, the entire MagPatch packaging was ensured to be autoclave compatible at 120 °C for sterilization.

C. Human neuroblastoma SHSY5Y cell line culture conditions

SHSY5Y is a human neuroblastoma cell line purchased from ATCC (CRL-2266) and cultured on the Parylene-C. The cells are cultured in the medium of a 1:1 mixture of Eagle's Minimum Essential Medium and F12 Medium plus 10% fetal bovine serum at 37 °C incubator with 5% CO_2. Before culturing the cells, the device substrates were sterilized by autoclave and double pre-coated with 5 μg/ml of recombinant human laminin for 3 days and then 5 μg/ml of fibronectin for 2 h.

D. Calcium imaging conditions

The cultured neuroblastoma cells were loaded with 10 μM Fluo-4 AM with PowerLoad (Thermo Fisher Scientific Life Sciences) in culture medium at 37 °C for 1 h. Following this, a perfusion chamber was affixed to the chip using vacuum grease (Corning). The cells were superfused continuously with extracellular medium containing 146 mM NaCl, 3 mM KCl, 2 mM $CaCl_2$, 2 mM $MgCl_2$, 1.25 mM NaH_2PO_4, 10 mM HEPES, 10 mM glucose, and 1 mM Na pyruvate (pH 7.4). Elevated potassium solutions (HiK) contained 80 mM KCl and 69 mM NaCl, as well as the other constituents listed above. All chemicals were purchased from Sigma-Aldrich. Glutamate HiK solutions were applied for 30–90 s via the superfusate by using a four-way valve to switch solutions.

The perfusion chamber was placed on the stage of an upright microscope (Olympus model BX51WI) (https://www.olympus-lifescience.com) equipped with a ×10 long working distance objective, a DG-4 fluorescence lamp and wavelength switcher (Sutter Instruments; Novato, CA, sutter.com), and an G:\Users\mapleshiao\Documents\Lab-work\Presentation\neuromodulation\Paultekintensified CCD video camera system (Paultek Imaging; Sunnyvale CA). MetaFluor imaging software (Molecular Devices, Sunnyvale, CA, http://www.moleculardevices.com) was used to acquire images at 1- to 2-s intervals, and Fluo-4 fluorescence intensity in regions of interest corresponding to cell bodies was plotted versus time using Microsoft Excel (Microsoft; Redmond, WA).

III. MODELING

A. FEM modeling of the microcoils in MagPatch array

Designing and fabricating new micromagnetic neurostimulators is challenging as it is difficult to predict their asymmetric

spatial E_{ind} field distributions. Even more challenging situations arise while designing arrays of μcoils. This is because, in addition to the E_{ind} distributions being spatially asymmetric, the E_{ind} field is also directional. This means the E_{ind} field from adjacent μcoils in an array either adds up or cancels out, depending on the direction of the current flowing through the μcoils. As neurostimulators, it is preferred that the E_{ind} field adds up for the designed μcoil arrays. This could contribute to reduced power requirements to drive these μcoils. Therefore, before fabricating such μcoil arrays as neurostimulators, one must study the spatial distributions of magnetic field (B-field) and induced electric field (E_{ind} field) profiles of these μcoils.

Owing to the micrometer size of these μcoils, it is difficult to experimentally measure the B-field and its corresponding E_{ind} field values. Previous attempts have been made using custom-made pick-up coils[5] and nitrogen-vacancy diamond magnetometers.[12] An extremely reliable and efficient method for understanding the B-field and E_{ind} field magnitudes and spatial distributions is through FEM.[2,3,25] In this work, we have used ANSYS-Maxwell[26] eddy current solver (ANSYS, Canonsburg, PA, USA) to design the MagPatch array implant. It solves a modified version of the T-Ω formulation of Maxwell's equations[27] to calculate the B-field and E_{ind} field values from the MagPatch arrays with the parameters described in Table I as the input. The entire modeling work was performed using the Minnesota Supercomputing Institute at the University of Minnesota (eight cores of Intel Haswell E5-2680v3 CPU, $64 \times 8 = 512$ GB RAM, and 1 Nvidia Tesla K20 GPU). The E_{ind} field values were later exported to be analyzed using a customized code written in MATLAB (The Mathworks, Inc., Natick, MA, USA).

B. NEURON modeling

Prior to the fabrication of the arrays, efforts were made to justify whether the MagPatch arrays designed through finite element modeling (see Sec. III A) would be successful in activating neurons. This led to a simulation study using the NEURON software.[21] The Layer 5 (L5) pyramidal neuron model was developed and reported by Pashut *et al.*[28] and has been modified to study the effect of the E_{ind} field from the MagPatch array. The spatial component of the E_{ind} field from the MagPatch array has been projected into a 3×3 mm^2 array in MATLAB by replacing the E_{ind} component in Pashut's NEURON model. Different positions of the pyramidal neuron were simulated relative to the center of the MagPatch array in the NEURON package.[21,29] The μcoils in the MagPatch array were modeled to be driven by a sinusoidal current of an amplitude of 2 A and a frequency of 2 kHz. The membrane potential at the soma of the pyramidal neuron model was then measured, and the volume of activation around the MagPatch array was estimated.

TABLE I. FEM modeling parameters for MagPatch array.

Parameter description	Value
Number of turns (N)	5
Wire diameter (b)	5 μm
Wire thickness (h)	2 μm
Distance between wires	5 μm
Surface area of the μcoil	190×190 μm^2
Distance between neighboring μcoils	600 μm
Tissue dimension (L × W × H)	3 mm × 3 mm × 300 μm
Conductivity of tissue (σ)	0.13 S/m
Relative permeability of tissue (μ_r)	1 (same as that of vacuum)
Air dimension (L × W × H)	$10 \times 10 \times 4$ mm^3
Energy error (user-specified)	%

IV. RESULTS AND DISCUSSION

A. Induced electric field (E_{ind}) from a single μcoil

The goal for the design of the MagPatch array was to facilitate cellular-level neuron activation. Numerical simulations on ANSYS-Maxwell (eddy current solver) (see Sec. III A) helped us identify the spatial distribution from each μcoil in the array measured on a tissue of dimension 3 mm × 3 mm × 300 μm at 20 μm from the μcoil surface. The μcoil was driving a sinusoidal current of 2 A at a frequency of 2 kHz. Our NEURON model (see Sec. III B) helped us identify if that μcoil design would successfully activate a single neuron. Figure 2(a) shows the spatial distribution of the induced electric field from a single planar μcoil. For a neuron situated at the location as shown in Fig. 2(a), our μcoil design showed successful activation as can be observed from the action potential plot in Fig. 2(b). Figures 2(c) and 2(d) show the x- and y-components of the induced electric field from each μcoil, respectively.

Our numerical modeling results helped us better realize the distance-dependent attenuation of the induced electric field. For a distance between the μcoil and the neural tissue greater than 20 μm [see Fig. 3(a)], the induced electric field value drops exponentially with an increase in distance [see Figs. 3(b) and 3(c)].

B. Design of array of μcoils for neurostimulation

The dimension of the individual planar μcoils being the same as in Fig. 1(c), we hereby arranged five of them in an array (see Fig. 4 and S3 in the supplementary material).[38] The simulation parameters remained the same as in Table I, the array arrangement of the μcoils was altered along with the direction of the current through them. Interestingly, for the same arrangement of the μcoil array, upon altering the direction of current through the μcoils [see solid-black arrows in Figs. 4(a-i)–4(c-i)], a completely different variant of the induced electric field spatial distribution was generated. In Fig. 4(a-i), for the same direction of the current through the five μcoils, the induced electric field spatially sums up at one end of the μcoil array. Just by reversing the direction of current in the second and the fourth μcoil in the array, another randomized spatial distribution of the induced electric field is generated [see Figs. 4(b-i) and 4(c-i)]. Furthermore, the directionality of the induced electric field had also altered [see white-solid arrows in Figs. 4(a-i)–4(c-i)]. In Fig. 4(a-i), the direction of the induced electric field causes it to sum up at one end. Whereas in Figs. 4(b-i) and 4(c-i), the directionality of the induced electric field changes due to the change in the direction of the current through the μcoils. The field from the third μcoil and the fourth μcoil in the array cancels each other at the center of the biological tissue [see Figs. 4(b-i)] resulting in zero induced electric field.

The x- and y-components of the induced electric field spatial distributions were calculated [see Figs. 4(a-i) and (a-iii) and 4(b-i)

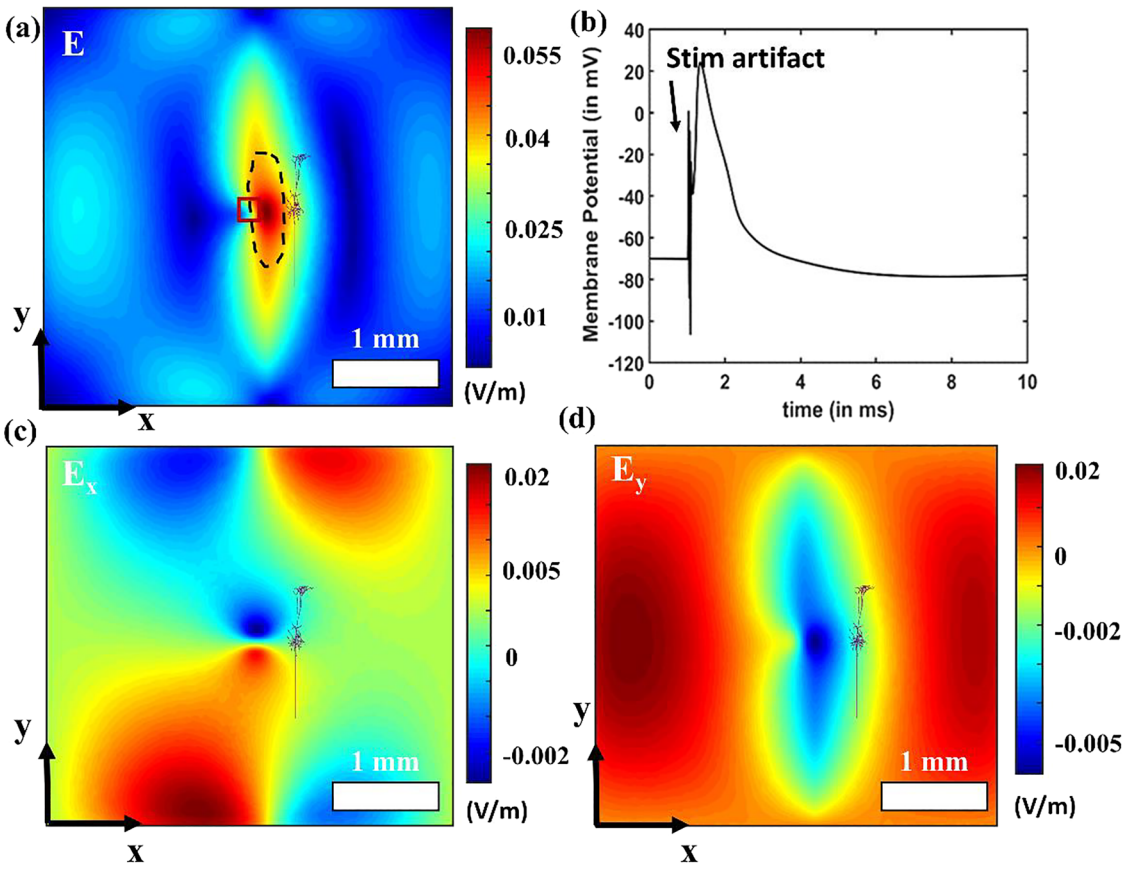

FIG. 2. FEM simulated electric field spatial contour maps from a single μcoil in the MagPatch array measured on a tissue of dimension 3 mm × 3 mm × 300 μm at 20 μm from the μcoil surface. (a) $\boldsymbol{E_{ind}}$ field spatial contour maps. The outer outline of the μcoil is shown in a solid square. The location of the neuron is shown. The maximum region where it can activate the neuron is shown in the dotted line. (b) The NEURON model simulated membrane potential from the neuron situated at the location on the tissue in Fig. 2(a). (c) E_x or x-component of the $\boldsymbol{E_{ind}}$ field spatial contour map. (d) E_y or y-component of the $\boldsymbol{E_{ind}}$ field spatial contour map. The μcoil was driven by a sinusoidal current of 2 A at a frequency of 2 kHz. E, E_x, and E_y are expressed in units of volt/meter (V/m).

and 4(b-iii)] and imported into the NEURON model to evaluate whether the combination could activate the neuron. For the arrangement and directionality of the μcoil array in Fig. 4(b), the location of the neuron as in Fig. 4(a) did not elicit an action potential [see Figs. 4(a-iii) and 4(b-iii)]. However, changing the location of the neuron as in Fig. 4(c) caused the neuron to fire [see Fig. 4(c-i)]. Other randomized arrangements of the μcoil array as in Fig. S3 show even more variation in the spatial distribution of the induced electric field and its directionality.

Therefore, variation in the arrangement of μcoil arrays in micromagnetic stimulation as well as the directionality of the current through them offer unique spatial induced electric field distributions. The arrangement of fascicles for a specific nerve can be determined and so can the orientation of nerve fibers in the brain. Therefore, for a known spatial arrangement of neurons, a careful design of an array of μcoils where the current driving individual μcoils can be controlled. This property can activate different sections of the nerve fascicle or even specific neuron fibers in the brain.

The arrangement of the μcoil array at the tip of the MagPatch device was an array in two rows [see Fig. S2(b) in S2 in the supplementary material].[38] This design for the two rows of μcoils has been validated using the laws of physics and our learnings from FEM modeling of μcoil array in Fig. 4. The fabricated MagPatch device has a common ground denoted by the "−" sign in Fig. 5. The other terminal of the μcoil is denoted as "+." Current through these μcoils flow from "+" to "−" terminal (denoted by solid-black arrows in Fig. 5). By right hand thumb/grip rule,[30] the direction of the magnetic field from the upper row of the μcoils will be in-plane (denoted by blue-"●" signs in Fig. 5) to the MagPatch device while that for the lower row of the μcoils will be out-of-plane (denoted by blue-"x" signs in Fig. 5). This magnetic field as per Faraday's laws of electromagnetic induction[31] induces an electric field which for an in-plane magnetic field is counter-clockwise while that for an out-of-plane magnetic field is clockwise (denoted by red arrows along the tangents of a white circle in Fig. 5). The μcoils in an array need to be arranged such that the direction of the induced

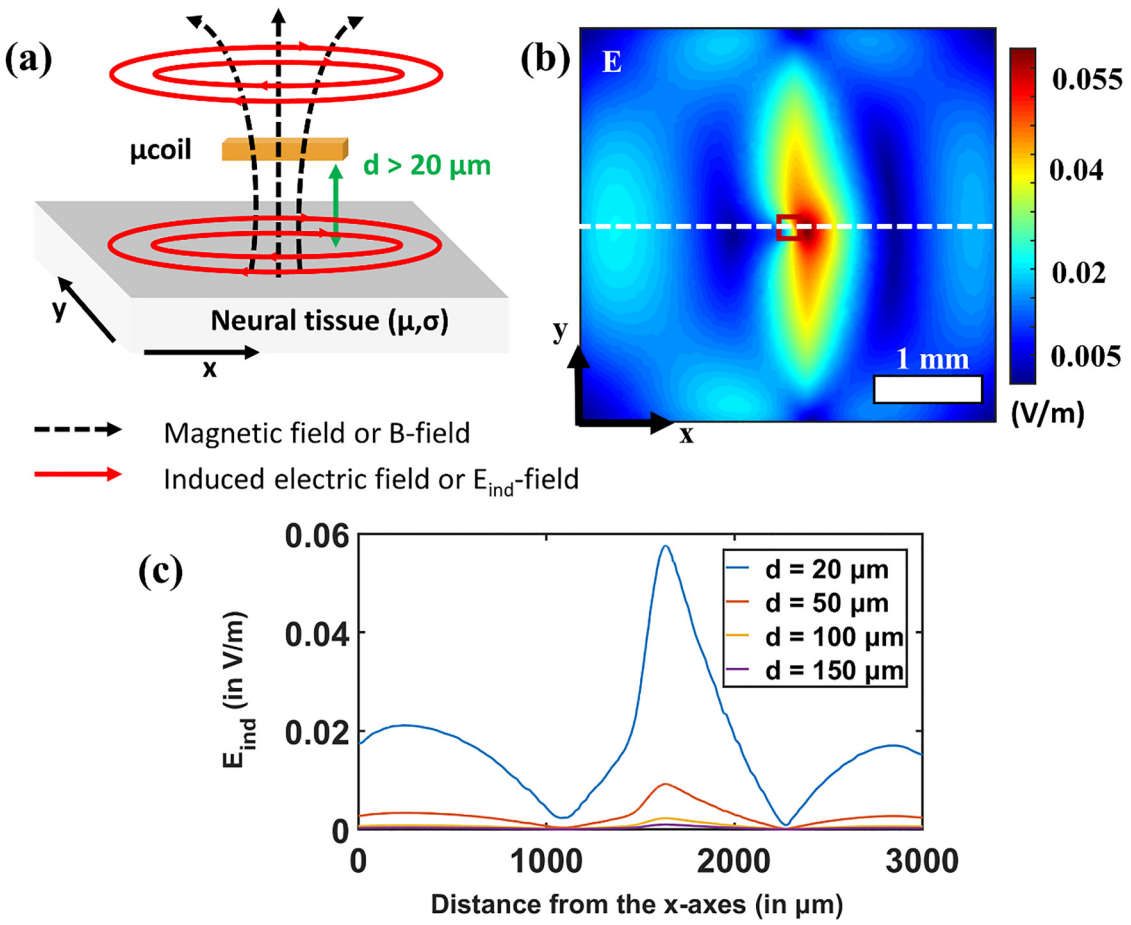

FIG. 3. Distance dependence of the MagPatch array's single μcoil. (a) Schematic figure of the single μcoil when the distance between the μcoil and the tissue (d) is greater than 20 μm. (b) The induced electric field value measured along *x* axis, across the dotted line. The outer diameter of the μcoil is shown in a solid square. (c) With an increase in distance between the μcoil and the neuron tissue beyond 20 μm, it was observed that the induced electric field value decreases drastically. The μcoil was driving a sinusoidal current of 2 A at a frequency of 2 kHz. *E* is expressed in units of volt/meter (V/m).

electric field from each of these μcoils in the array ultimately sums up and does not cancel each other (see the two big red arrows in Fig. 5).

C. Scaling effects on electrical characteristics of the planar microcoil

The RLC characteristics of the MagPatch μcoil have been validated using numerical calculations[32] (see Fig. 6), simulations using Fast Field Solvers (https://www.fastfieldsolvers.com/) and experimentally using LCR meter measurements (see Table S1 in S4 in the supplementary material).[38] Each of the μcoil in the MagPatch array reduces to an RL||C (resistance and inductance in series but the capacitance in parallel) circuit (see details in S4 in the supplementary material and Fig. 6).[38] The eight μcoils in the MagPatch array are connected by common ground, hence their circuit equivalent reduces to Fig. S4.

During the design of an implant, a thorough study of the effects of scaling its dimensions on its electrical parameters is required. The reason is that an implant modeled and designed for a rodent's brain needs to be scaled up for testing on non-human primates and ultimately on humans. As reported by Neagu *et al.*,[32] altering the dimensions of a μcoil alters the resistance, inductance, and capacitance of the μcoil. In this work, we have primarily studied the effect of the wire width (*b*), wire thickness (*h*), and outer diameter (*D*) of the μcoil [see Fig. 6(a)]. The *D* is directly related to the number of turns of the μcoil and hence the total length (*l*) of the μcoil. The DC resistance (R_{DC}) of the planar μcoil is given by

$$R_{DC} = \frac{\rho^{\star} L}{b^{\star} h}, \tag{1}$$

where ρ is the specific resistivity of the material of the μcoil (in this case it is gold, $\rho_{Au} = 0.22\ \mu\Omega$ m) and *L* is the length of the μcoil.

The series inductance (L_s) of the planar μcoil is expressed as[32]

$$L_s = \left(\frac{2\mu D}{\pi}\right) N^2 \left[\ln\left(\frac{4D}{Np}\right) + 0.894\left(\frac{Np}{4D}\right) - 0.66 - \frac{A+B}{N}\right], \quad (2)$$

where $N$is the number of turns of the μcoil, $p = x + b$, and x = spacing between two adjacent turns. A and B are constants for the μcoil depending on wire width and wire spacing. For $N < 10$ and when $0.3p < b < 0.8p$, $A = 2[(b/p) - 0.6]$ and $B = 0.0336$*N.

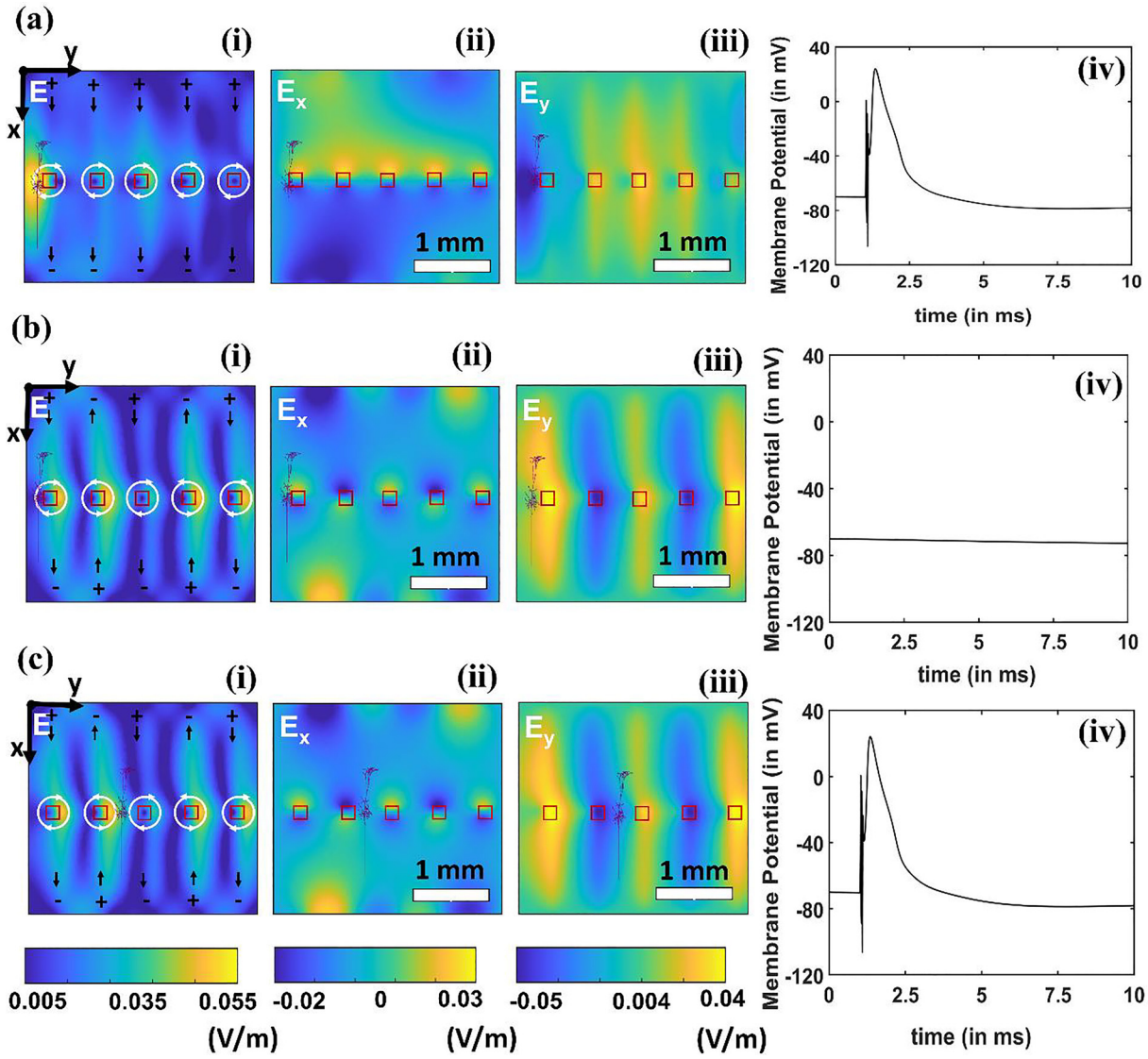

FIG. 4. Spatial contour plots of induced electric field (E) for an array of five planar μcoils measured on a tissue of dimension 3 mm × 3 mm × 300 μm. The separation between tissue and the μcoils is 20 μm. The outline of μcoils is shown in solid squares. The directionality of the induced electric field is shown in solid circles. The direction of the current through the μcoils is shown in solid arrows. (a) The current driving each planar μcoil is along the same direction. (i) E in V/m and (ii) x-component of the induced electric field (E_x in V/m). (iii) y-component of the induced electric field (E_y in V/m). (iv) For the location of a neuron on the tissue, the generated action potential along the neuron membrane. (b) The current driving each planar μcoil is not along the same direction—μcoils in the second and fourth position in the array have opposite current directions compared to the other μcoils in the array. (i) E in V/m, (ii) E_x in V/m, and (iii) E_y in V/m. (iv) For the location of a neuron on the tissue, no action potential was generated along the neuron membrane. (c) The current driving each planar μcoil is not along the same direction—μcoils in the second and fourth position in the array have opposite current direction compared to the other μcoils in the array. (i) E in V/m, (ii) E_x in V/m, and (iii) E_y in V/m. (iv) For the location of a neuron on the tissue, the generated action potential along the neuron meme. E, E_x, and E_y are expressed in units of volt/meter (V/m).

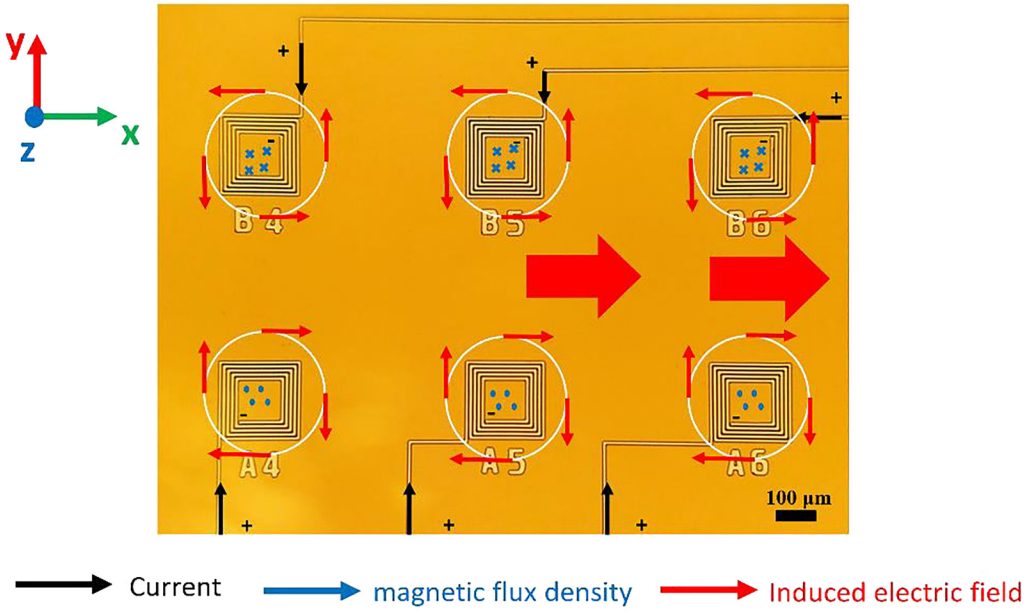

FIG. 5. Validation of the design of a two row µcoil array at the tip of the MagPatch array device using right hand thumb/grip rule and Faraday's laws of electromagnetic induction. This pictorially shows the direction of current (see solid arrows from "+" to "–"), magnetic field (see —"●" and "x" signs), and induced electric field (see solid arrows around the circle) from each of these µcoils in the MagPatch array.

Finally, the parallel capacitance (C_p) is contributed by the thickness of the Au and Si_3N_4 layers stacked. In this work, we have considered two capacitances contributed by the Au layer (C_{Au}) that forms the common ground for MagPatch and the Si_3N_4 layer (C_{SiN}) that forms the passivation layer for MagPatch to be in parallel. Hence, the total parallel capacitance (C_p) for MagPatch (considering other capacitive effects to be negligible) has been calculated as

$$C_p = C_{Au} + C_{SiN}, \tag{3}$$

where $C_{Au} = \frac{\epsilon_{Au} bh}{d_{Au}}$, $C_{SiN} = \frac{\epsilon_{SiN} bh}{d_{SiN}}$, $\varepsilon_{Au} = 1.6$ (relative permittivity of Au), $\varepsilon_{SiN} = 8$ (relative permittivity of Si_3N_4), $d_{Au} = 2.1\,\mu$m (thickness of the Au layer), and $d_{SiN} = 100$ nm (thickness of the Si_3N_4 layer).

Ideally for a micromagnetic implant, the electrical characteristics must be reduced to a series RL circuit.[2] Therefore, the C_p that arises for the µcoils in MagPatch needs to be minimal. This will cause the impedance $\left(\frac{1}{wC_p}\right)$ to be high enough to block the flow of current I_c through C_p branch. Then, the electrical characteristics of the µcoil in the MagPatch array will tend more toward a series RL circuit. It is desirable for these µcoils to have a higher series inductance (L_s) as it contributes to a greater induced electric field value. Furthermore, a lower DC resistance (R_{DC}) contributes to lower thermal effects on neural tissue, hence it is more desirable (see S5 in the supplementary material).[38]

With an increase in h value for the planar µcoil, R_{DC} and L_s values decrease whereas C_p values increase [see Figs. 6(c-i) and 6(c-iv)]. With an increase in b for the planar µcoil, R_{DC}, L_s, and C_p values decrease [see Figs. 6(c-i) and 6(c-v)]. An increase in the outer diameter (D) of the µcoil causes R_{DC}, L_s, and C_p values to increase [see Figs. 6(c-i) and 6(c-vi)]. In summary, increased wire width and wire thickness coupled with the small outer diameter of the µcoil contributes to a desirable R_{DC}. A decreased wire width and wire thickness with a large outer diameter of the µcoil contributes to desirable L_s. To reduce the C_p value, an increased wire thickness, reduced wire width and small outer diameter will be desired. Hence, there is a trade-off affecting electrical characteristics while scaling these µcoils to fit different applications. The frequency for L_s and $\mathbf{C_p}$ calculations has been kept constant at 1 kHz. The impact of scaling h, b, and D parameters of the µcoil on the quality factor (Q) of the µcoil, heat energy released, and change in tissue temperature upon µcoil operation has been discussed in S5 in the supplementary material.[38]

D. Strength-frequency curve for a µcoil in MagPatch array

The neurostimulation effect from µcoils has been controversial in the literature. Due to the high current requirements for these µcoils, some researchers argue the neural activation from these µcoils is an effect of Joule heating of these µcoils.[33] However, in our study on micromagnetic activation of the rat sciatic nerve,[3] we reported a dose-response relationship for micromagnetic stimulation. The highlight of this relationship was that at higher

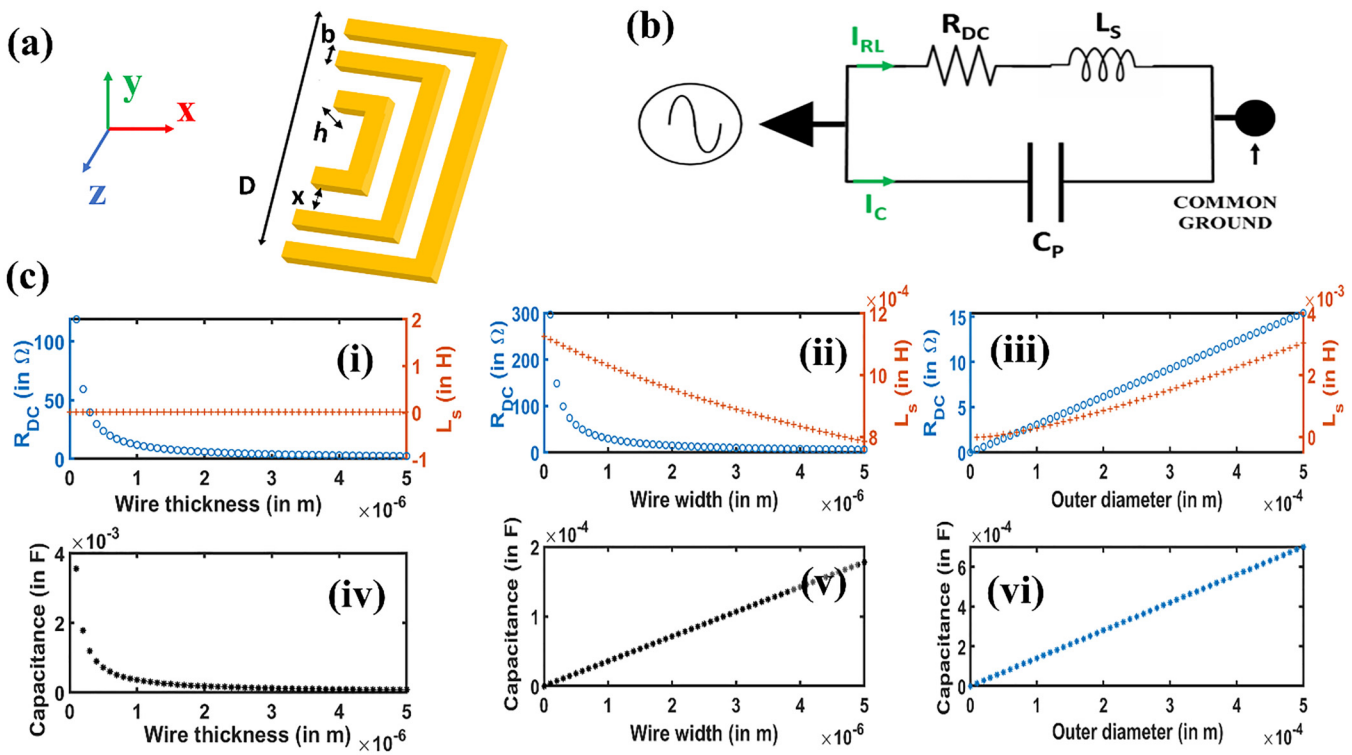

FIG. 6. (a) Schematic of the planar μcoil dissected along the *z* axis to pictorially demonstrate the wire width of the μcoil (along the *y* axis), wire thickness of the μcoil (along the *z* axis), and outer diameter of the μcoil (*D*). (b) The electrical characteristics of a single μcoil in a MagPatch array reduce to an RL||C circuit. The current gets divided into two branches: one through the resistor and the inductor in series (I_{RL}) and the other through the capacitor in parallel to the resistor and the inductor (I_c). (c) Scaling effects on R_{DC}, L_s, and C_p through numerical calculations. (i) R_{DC} and L_s decrease exponentially with an increase in wire thickness (*h*) of the μcoil. (ii) R_{DC} and L_s decrease exponentially with an increase in wire width (b) of the μcoil. (iii) R_{DC} and L_s increase exponentially with an increase in the outer diameter (*D*) of the μcoil which corresponds to the number of turns in the μcoil. (iv) C_p decreases exponentially with an increase in wire thickness (*h*) of the μcoil. (v) C_p increases linearly with an increase in wire width (*b*) of the μcoil. (vi) C_p increases exponentially with an increase in the outer diameter (*D*) of the μcoil which corresponds to the number of turns in the μcoil.

frequencies, the current required to drive these μcoils for neurostimulation was reduced. This follows directly from Faraday's law of electromagnetic induction where the induced electric field which activates the neurons is directly proportional to the frequency of the current driving the μcoils.

In this work, the μcoils in the MagPatch array also follow a similar trend. Using the induced electric field spatial contour plots from these μcoils generated from ANSYS in our NEURON model, we investigated the minimum current amplitude at a particular frequency required to drive a μcoil to activate a neuron. With an increase in frequency, the current required to drive the μcoil reduces (see Fig. 7). However, unlike our MagPen prototype,[2] this reduction in current amplitude with the increase in frequency stops after 3 kHz. For μcoils driving current above 3 kHz frequency, the current amplitude requirement starts increasing (see Fig. 7). This is because a neuron acts like a low pass filter (LPF) and it cannot register a stimulus beyond a certain frequency.[34–36] At those higher frequencies to exhibit neurostimulation, a higher amplitude of current is required to drive the μcoils.

E. Adhesion of SHSY5Y human neuroblastoma cell line with Parylene-C

The MagPatch was encapsulated using Parylene-C and human neuroblastoma cells SHSY5Y were cultured as described in Sec. II E. The adhesion of the neuroblastoma cells was variable for the ten independent trials. On one occasion when the cells were well attached to the device [see Fig. 8(a)], calcium imaging experiments were conducted to assess the viability of the cells in the MagPatch environment. Intracellular calcium concentration increased in multiple cells after the perfusate was switched to HiK, and returned to baseline after the perfusate was switched back to control medium. This response to depolarization with HiK demonstrated that the neuroblastoma cells were viable and functional [see Fig. 8(b)].

F. Discussions

Electrical characterization of each μcoil in the MagPatch array showed that the μcoil reduces to an RL||C circuit. However, for optimal neurostimulation performance,[2,3] it is desirable for

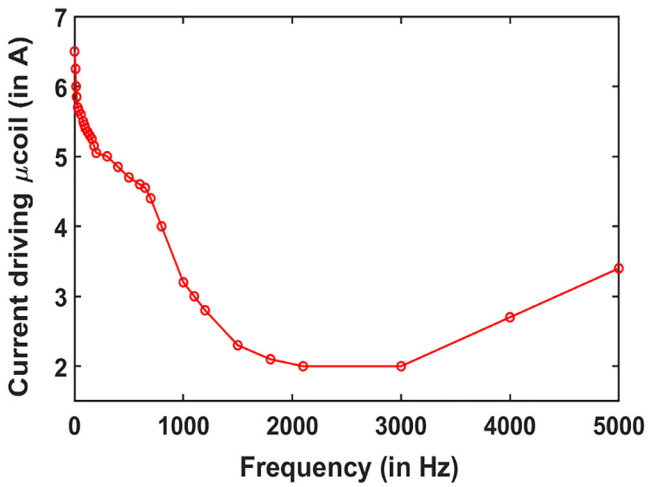

FIG. 7. Strength-frequency curve for a single planar μcoil in the MagPatch array.

micromagnetic neurostimulation implants to reduce to that of a series RL circuit. This means an additional reduction of C_p will be necessary for future MagPatch designs. Research reported in this work shows techniques by which we can address this issue. For instance, increasing the wire thickness (h) leads to a desirable reduction in both R_{DC} as well as C_p [see Figs. 6(c-i) and 6(c-iv)]. But, there lies a trade-off—the aspect ratio of the wire width and wire height (b:h) is limited. An extremely thick wire may cause the structure to topple. Similarly, reducing the wire width (b) favors the increase in L_s and reduction in C_p [see Figs. 6(c-i) and 6(c-v)] but there needs to be a trade-off as R_{DC} increases significantly contributing to increased thermal effects on neural tissues [see Figs. S5 (b-ii) and S5(b-iii) in the supplementary material]. Finally, a reduction in the outer diameter (D) of the μcoil favors a reduction in R_{DC} and C_p [see Figs. 6(c-i) and 6(c-vi)] but causes an undesirable decrease in L_s [Fig. 6(c-i)]. Therefore, a study on the impact of the scaling effect on these μcoils suggests that there will always be a trade-off while designing μcoils for micromagnetic stimulation. But to meet our goal of cellular-level neurostimulation, designing the μcoils in the MagPatch array with $b = 5\,\mu m$, $h = 2\,\mu m$ and $D = 190\,\mu m$ was optimum. These dimensions led to the RLC characteristics reported in Table S1 and an optimum Q-factor for μMS that is like that of MagPen[2,3] ($Q \sim 0.02$).

Further reduction of C_p could probably be achieved by removing the common ground for the μcoil array (each μcoil will have its independent ground) and reducing the MagPatch fabrication to a one-step photolithography process. However, this may or may not have consequences on other electrical parameters, R_{DC} and L_s, which will need further investigation. The frequency-dependent operation for the μcoils in the MagPatch array corroborates the dose-response curve for μMS experimentally reported on the rat sciatic nerve.[2] Therefore, it is true that increasing the frequency of the micromagnetic stimulus reduces the amplitude of the current required to drive the μcoil for neurostimulation. However, the strength-frequency curve reported in Fig. 7 shows that one cannot keep on increasing the frequency of the micromagnetic stimulus in hopes of reducing the power requirements. This is because neurons behave as LPFs and block extremely high frequency stimuli.[34–36] All our experimental works have taken this fact into consideration while designing the μcoil driving waveform. Designing arrays of μcoils to facilitate μMS is a new topic and this work shows how a careful arrangement of μcoils can help increase the induced electric field magnitude, thereby reducing the power consumption for the μcoils in the array (see Sec. IV B).

The MagPatch array has been designed as per "The Pentagon for Implant Design Constraints" reported in Ref. 20. We have ensured a basic biocompatibility by fabricating the prototype out of Ti, Au, and Si_3N_4 (see Sec. II A). Each μcoil in the array has an outer dimension of $190 \times 190\,\mu m^2$ which is small enough to

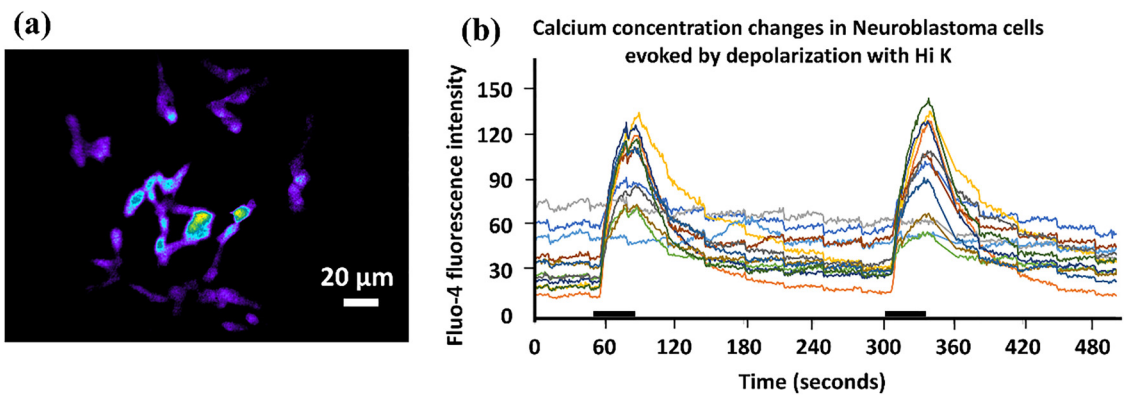

FIG. 8. (a) SHSY5Y human neuroblastoma cells cultured on Parylene-C encapsulation loaded with Ca^{2+} ion staining dye Fluo-4. (b) Calcium concentration changes recorded from the neuroblastoma cells cultured on Parylene-C that were depolarized using HiK, an external chemical stimulus. The black bars indicate the time during which the perfusion was switched to the HiK solution. Each colored line on the graph of (b) represents the fluorescence signal recorded over time from a single cell in the image in (a).

facilitate single neuron activation, thereby improving accessibility to the implantation site. The MagPatch is encapsulated in Parylene-C, a water-tight, biocompatible, and insulating coating which ensures that the nature of neurostimulation from these μcoils is primarily micromagnetic and not an effect of leakage current (see Sec. II B). Finally, as these μcoils activate the neurons using an induced electric field, there is no electrochemical contact with the neural tissues contributing to minimal implant site nuances. Thus, we have verified four vertices of "The Pentagon for Implant Design Constraints." The fifth vertex is the fabrication of the implant on a flexible substrate whose Young's modulus is comparable to that of the brain tissue. This constraint for implant design will be considered for future MagPatch designs where we will investigate *in vivo* demonstration of the μcoil array design. That will also be when one needs to seriously investigate the scaling effects of the μcoil design as reported in Sec. IV C. This work investigates biocompatibility of MagPatch at a very basic level. Although the components of MagPatch, Au, Ti, Si_3N_4, and Parylene-C are all extensively used in state-of-art biomedical implants, the entire MagPatch device needs to undergo comprehensive biocompatibility testing as per ISO 10993 standards.[37] The future goal for further development of MagPatch implant will involve extensive immunohistochemistry staining assays which will provide us valuable information on the different levels of cell necrosis, inflammation, white matter damage, glial cell formation, etc.

V. SUMMARY AND CONCLUSIONS

The design, fabrication, and testing of MagPatch, the rectangular helix-shaped planar μcoil array prototype is a pioneering report where the importance of directionality of the $\boldsymbol{E_{ind}}$ field from each μcoil in the array for spatially selective neurostimulation was investigated. The MagPatch array prototype has been designed using FEM modeling and the single neuron activation capability has been established using a custom-developed NEURON model. The designed μcoil array had been fabricated on silicon substrates using three biocompatible materials—Ti, Au, and Si_3N_4—following the principles of "The Pentagon for Implant Design Constraints." The final MagPatch prototype has been encapsulated in Parylene-C as the water-tight, biocompatible, and anti-leakage current coating to ensure the stimulation effect from these μcoils is completely micromagnetic in nature. A basic biocompatibility of the MagPatch prototype was experimentally proved by culturing human neuroblastoma SHSY5Y cell line on the Parylene-C coated with laminin and fibronectin. After adhering to the device, the cells responded to the HiK stimulus implying they were alive in the MagPatch environment. Finally, a detailed study on the scaling effects of the wire width, wire thickness, and outer diameter of μcoil in the MagPatch array inferred that custom designing larger μcoils to fit *in vivo* applications in non-human primates and ultimately humans will have consequences. Scaling the μcoils will impact the electrical characteristics of the μcoil, thermal effects on the neural tissues, and even the Q-factor of the μcoil. The strength-frequency curve generated from the designed μcoils in MagPatch corroborates the frequency-dependent nature of activation in micromagnetic neurostimulation. However, the fact that a lower amplitude of the current is required to activate neurons when the current is of a higher frequency is limited up to a certain frequency since neurons act as low-pass filters. Additionally, in future, a comprehensive biocompatibility testing on the MagPatch device needs to be performed as per ISO 10993 standards to find this prototype's potential as a successful biomedical implant.

ACKNOWLEDGMENTS

This study was financially supported by the Minnesota Partnership for Biotechnology and Medical Genomics under Award No. ML2020 (Chap 64. Art I, Sec. 1.4). R.S. acknowledges the three-year College of Science and Engineering (CSE) fellowship awarded by University of Minnesota, Twin Cities. Research reported in this publication was supported by the University of Minnesota's MnDRIVE (Minnesota's Discovery, Research and Innovation Economy) initiative. The authors would also like to thank Winfried A. Raabe, M.D. from the Department of Neurosurgery and Kendall H. Lee, M.D., Ph.D., Charles D. Blaha, Ph.D., and Yoonbae Oh, Ph.D. from Mayo Clinic, Rochester, MN for useful discussions. Portions of this work were conducted in the Minnesota Nano Center (MNC), which is supported by the National Science Foundation through the National Nano Coordinated Infrastructure Network (NNCI) under Award No. ECCS-2025124. J.-P.W and R.S. also thank the Robert Hartmann Endowed chair support.

AUTHOR DECLARATIONS

Conflict of Interest

The authors have no conflict to disclose.

Author Contributions

Renata Saha: Conceptualization (equal); Data curation (equal); Formal analysis (equal); Investigation (equal); Methodology (equal); Software (equal); Validation (equal); Visualization (equal); Writing – original draft (equal); Writing – review & editing (equal). **Onri J. Benally:** Methodology (supporting). **Sadegh Faramarzi:** Software (equal). **Robert Bloom:** Methodology (supporting). **Kai Wu:** Funding acquisition (supporting); Methodology (supporting); Writing – review & editing (supporting). **Denis Tonini:** Methodology (supporting); Writing – review & editing (supporting). **Maple Shiao:** Data curation (equal); Investigation (equal); Methodology (equal); Writing – review & editing (supporting). **Susan A. Keirstead:** Formal analysis (equal); Investigation (equal); Methodology (equal); Resources (equal); Software (equal); Supervision (lead); Validation (equal); Visualization (equal); Writing – review & editing (equal). **Walter C. Low:** Conceptualization (equal); Funding acquisition (equal); Investigation (equal); Methodology (equal); Supervision (lead); Validation (equal); Writing – review & editing (supporting). **Theoden I. Netoff:** Conceptualization (equal); Funding acquisition (equal); Investigation (equal); Methodology (equal); Supervision (lead); Writing – review & editing (supporting). **Jian-Ping Wang:** Conceptualization (equal); Funding acquisition (equal); Investigation (equal); Supervision (equal); Visualization (equal); Writing – review & editing (equal).

DATA AVAILABILITY

The data that support the findings of this study are available from the corresponding author upon reasonable request.

REFERENCES

[1]G. Bonmassar, S. W. Lee, D. K. Freeman, M. Polasek, S. I. Fried, and J. T. Gale, Nat. Commun. **3**, 921 (2012).
[2]R. Saha *et al.*, J. Neural Eng. **19**, 016018 (2022).
[3]R. Saha *et al.*, J. Neural Eng. **20**, 036022 (2023).
[4]S. W. Lee, F. Fallegger, B. D. Casse, and S. I. Fried, Sci. Adv. **2**, e1600889 (2016).
[5]S. Minusa, H. Osanai, and T. Tateno, IEEE Trans. Biomed. Eng. **65**, 1301 (2018).
[6]S. Minusa, S. Muramatsu, H. Osanai, and T. Tateno, J. Neural Eng. **16**, 066014 (2019).
[7]H. Ye and L. Barrett, Sci. Rep. **11**, 1 (2021).
[8]J. Skach, C. Conway, L. Barrett, and H. Ye, Sci. Rep. **10**, 1 (2020).
[9]R. Saha, K. Wu, and J.-P. Wang, *2023 11th International IEEE/EMBS Conference on Neural Engineering (NER)*, Baltimore, MD, 24–27 April 2023 (IEEE, New York, 2023), pp. 1–4.
[10]M.-E. Rizou and T. Prodromakis, Biomed. Phys. Eng. Express **4**, 025016 (2018).
[11]H. Jeong, J. Deng, and G. Bonmassar, J. Vac. Sci. Technol. B **39**, 063202 (2021).
[12]A. Khalifa *et al.*, Microsyst. Nanoeng. **7**, 1 (2021).
[13]S. W. Lee and S. I. Fried, *2014 36th Annual International Conference of the IEEE Engineering in Medicine and Biology Society*, Chicago, IL, 26–30 August 2014 (IEEE, New York, 2014), pp. 6125–6128.
[14]S. W. Lee and S. I. Fried, *2015 7th International IEEE/EMBS Conference on Neural Engineering (NER)*, Montpellier, France, 22–24 April 2015 (IEEE, New York, 2015), pp. 268–271.
[15]M. Alzahrani and B. J. Roth, IEEE Trans. Biomed. Eng. **70**, 3260 (2023).
[16]B. Cao, Y. Zheng, T. Xi, C. Zhang, W. Song, K. Burugapalli, H. Yang, and Y. Ma, Biomed. Microdevices **14**, 709 (2012).
[17]E. T. Demann, P. S. Stein, and J. E. Haubenreich, J. Long Term Eff. Med. Implants **15**, 687 (2005).
[18]T. J. Webster, A. A. Patel, M. Rahaman, and B. S. Bal, Acta Biomater. **8**, 4447 (2012).
[19]K. Wang, Mater. Sci. Eng. A **213**, 134 (1996).
[20]E. McGlynn, V. Nabaei, E. Ren, G. Galeote-Checa, R. Das, G. Curia, and H. Heidari, Adv. Sci. **8**, 2002693 (2021).
[21]M. L. Hines and N. T. Carnevale, Neural Comput. **9**, 1179 (1997).
[22]K. R. Williams, K. Gupta, and M. Wasilik, J. Microelectromech. Syst. **12**, 761 (2003).
[23]C. Hassler, R. P. von Metzen, P. Ruther, and T. Stieglitz, J. Biomed. Mater. Res. B **93**, 266 (2010).
[24]S. van den Driesche, C. Habben, A. Bödecker, W. Lang, and M. J. Vellekoop, Proceedings **1**, 299 (2017).
[25]L. Golestanirad, J. T. Gale, N. F. Manzoor, H.-J. Park, L. Glait, F. Haer, J. A. Kaltenbach, and G. Bonmassar, Front. Physiol. **9**, 373586 (2018).
[26]A. S. Martyanov and N. I. Neustroyev, Eastern Eur. Sci. J. **5** (2014), http://journale.auris-verlag.de/index.php/EESJ/article/view/231.
[27]Z. Ren, IEEE Trans. Magn. **38**, 557 (2002).
[28]T. Pashut, S. Wolfus, A. Friedman, M. Lavidor, I. Bar-Gad, Y. Yeshurun, and A. Korngreen, PLoS Comput. Biol. **7**, e1002022 (2011).
[29]N. T. Carnevale and M. L. Hines, *The NEURON Book* (Cambridge University, London, 2006).
[30]E. Özdemir and M. Çoramık, J. Balt. Sci. Ed. **17**, 320 (2018).
[31]I. Galili, D. Kaplan, and Y. Lehavi, Am. J. Phys. **74**, 337 (2006).
[32]C. R. Neagu, H. V. Jansen, A. Smith, J. G. E. Gardeniers, and M. C. Elwenspoek, Sens. Actuators A **62**, 599 (1997).
[33]T. Kim, H. Kadji, A. J. Whalen, A. Ashourvan, E. Freeman, S. I. Fried, S. Tadigadapa, and S. J. Schiff, J Neural Eng. **19**, 056029 (2022).
[34]I. Parnas, S. Hochstein, and H. Parnas, J. Neurophysiol. **39**, 909 (1976).
[35]R. Wang, C. Jin, A. McEwan, and A. van Schaik, *2011 IEE International Symposium of Circuits and Systems (ISCAS)*, Rio de Janeiro, Brazil, 15–18 May 2011 (IEEE, New York, 2011), pp. 869–872.
[36]C. M. Zierhofer, IEEE Trans. Biomed. Eng. **48**, 173 (2001).
[37]R. F. Wallin and E. Arscott, Med. Device Diagn. Ind. **20**, 96 (1998).
[38]See the supplementary material (S1–S5) online for the fabrication flowchart for the MagPatch arrays, packaging and electrical interface for MagPatch along with scanning electron microscope (SEM) images of the microcoil arrays, the design of microcoil array for neurostimulation, the electrical circuit equivalent of the microcoil in the MagPatch array, and scaling effects on the Q factor of the microcoil, heat energy released, and change of temperature in the tissue.